Supplementary Information

Ammonium Vanadium Oxide Nanobelt-Integrated Sulfur Hosts Enabling Enhanced Polysulfide Redox Kinetics in Lithium–Sulfur Batteries

Kiseok Lee,†[a] Eun Ji Lee,†[a] Hyung-Kyu Lim,*[b] Ji Eun Lee*[a]

[a]*Department of Chemical Engineering, Chonnam National University, Gwangju 61186, Republic of Korea. E-mail: jelee@jnu.ac.kr*

[b]*Department of Chemical Engineering and Bioengineering, Kangwon National University, Chuncheon 24341, Republic of Korea. E-mail: hklim@kangwon.ac.kr*

Supporting Figures

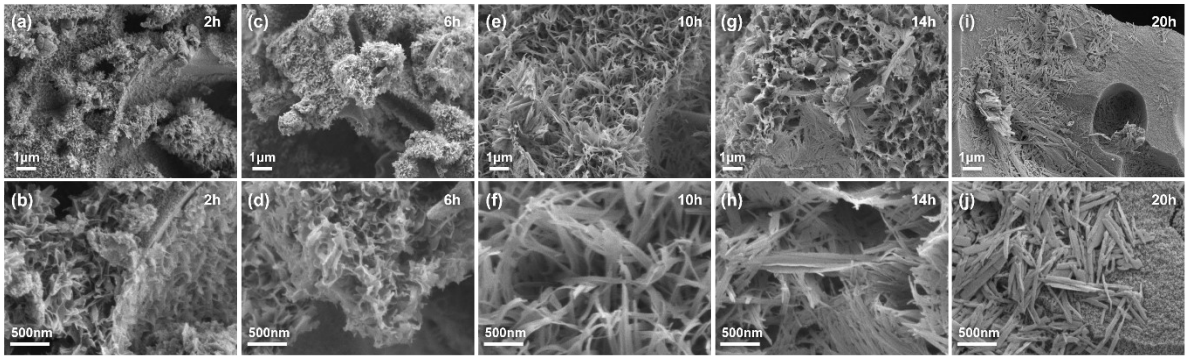

Fig. S1 SEM Images of NVO/AC composites synthesized at different hydrothermal reaction times: (a, b) 2h, (c, d) 6h, (e, f) 10h, (g, h) 14h, (i, j) 20h.

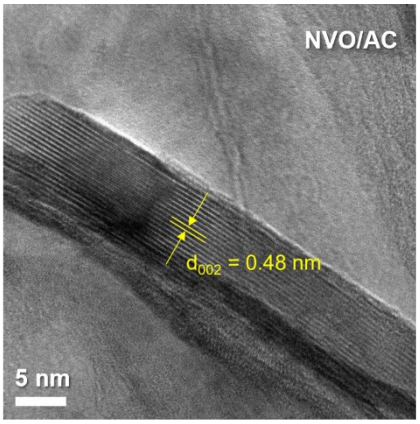

Fig S2. TEM image of NVO/AC.

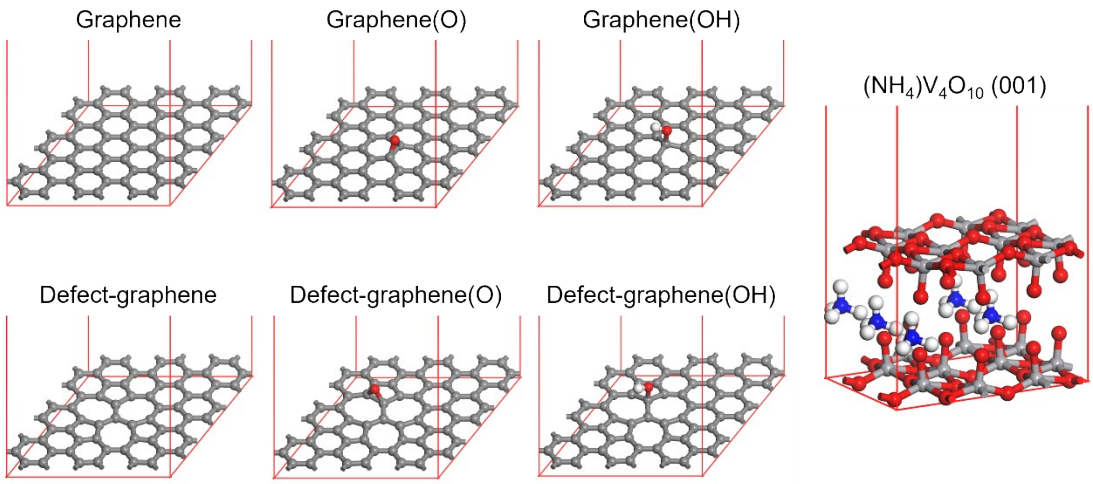

Fig. S3. Optimized surface models used in the DFT calculations: pristine graphene, graphene with adsorbed oxygen (*O), graphene with adsorbed hydroxyl (*OH), defect-graphene, defect-graphene with *O, defect-graphene with *OH, and the $(NH_4)V_4O_{10}$ (001) surface.

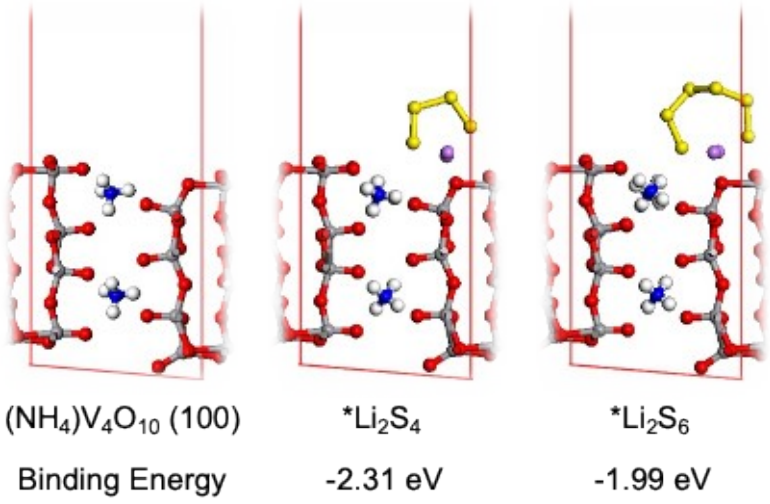

Fig. S4. DFT results for Li_2S_4 and Li_2S_6 adsorption on the NVO (100) surface.

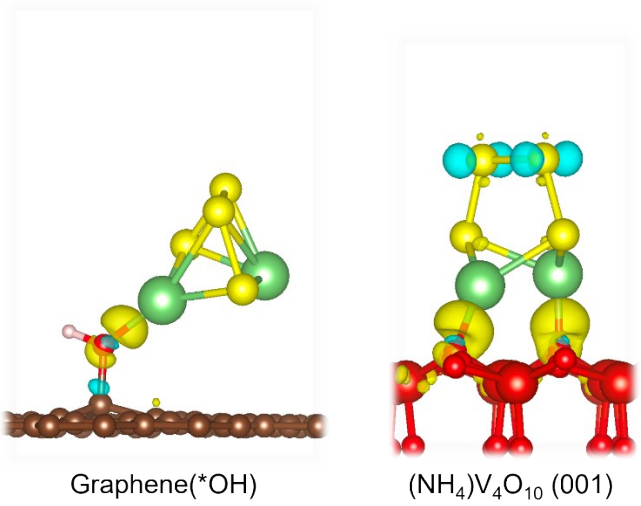

Fig. S5. Differential charge density plots for Li_2S_4 adsorbed on (left) the graphene(*OH) surface and (right) the NVO (001) surface. Yellow and cyan isosurfaces represent electron accumulation and depletion regions, respectively (isosurface level = 0.005 *e*/Å^3).

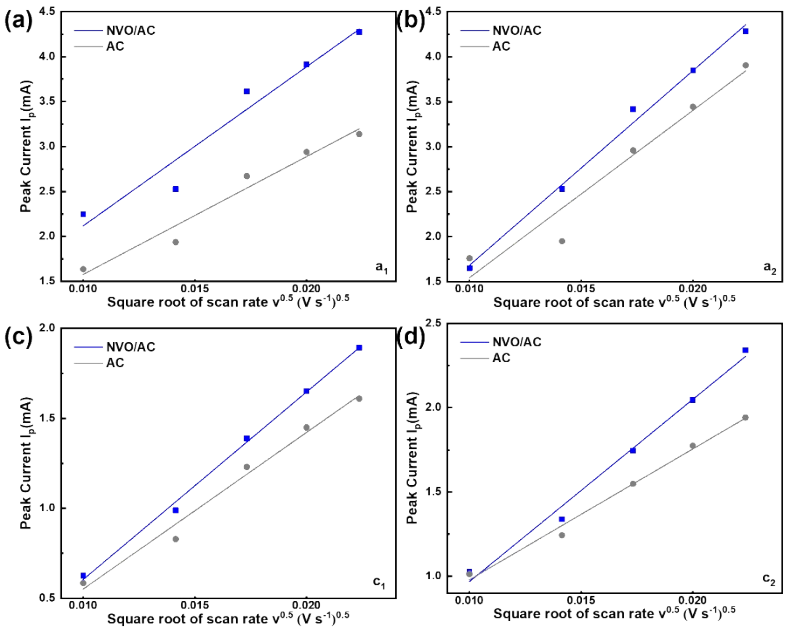

Fig. S6 Linear relationship between anodic and cathodic peak currents and the square root of the scan rate obtained from CV analysis.

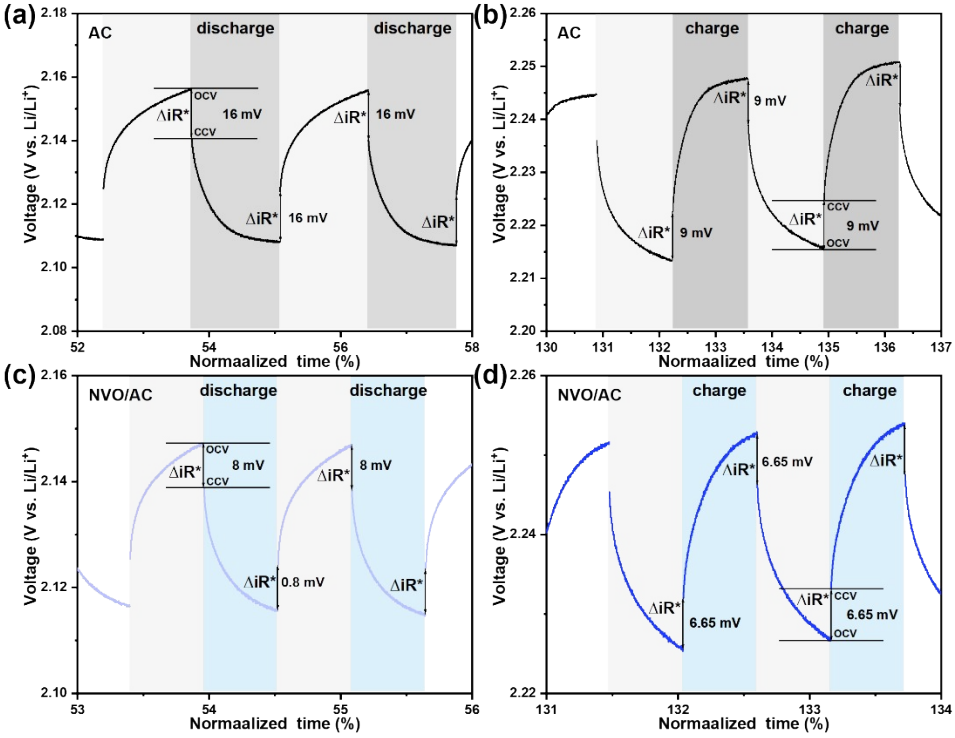

Fig. S7 Enlarged GITT plots of (a, b) AC and (c, d) NVO/AC.

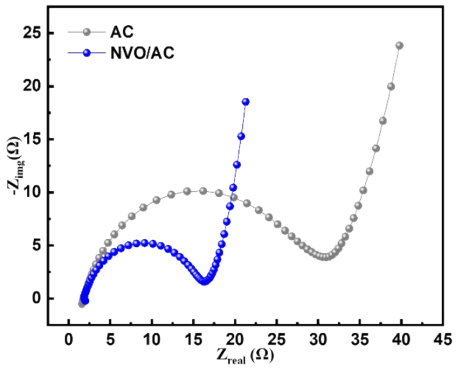

Fig. S8 Nyquist plots comparing the resistance of AC and NVO/AC.

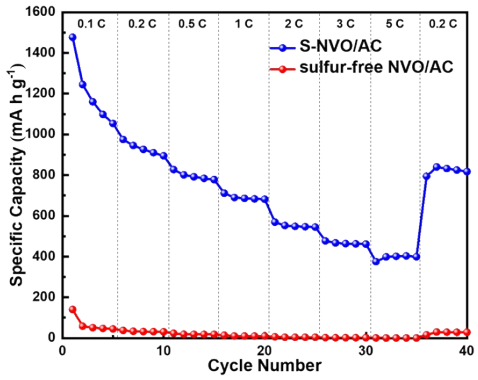

Fig. S9. Rate performance of NVO/AC with and without sulfur loading at various C-rates.

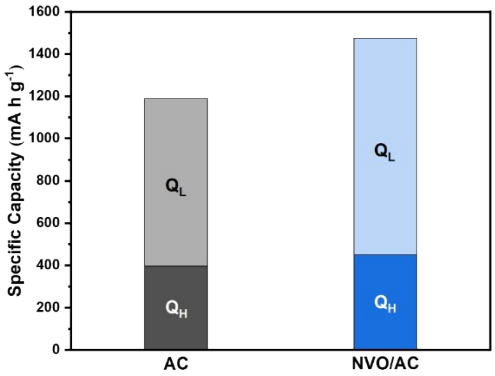

Fig. S10 Higher plateau capacity (Q_H) and lower plateau capacity (Q_L) of AC and NVO/AC from initial discharge profiles at 0.1 C.

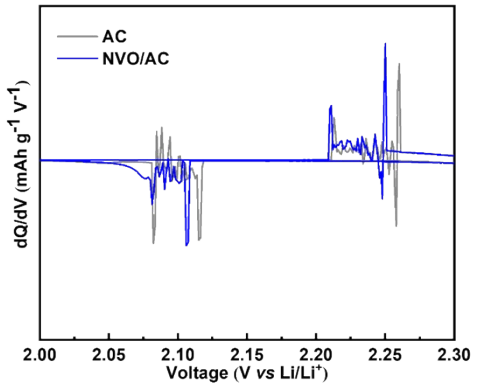

Fig. S11 Differential capacity (dQ/dV) profiles from initial charge–discharge of AC and NVO/AC.

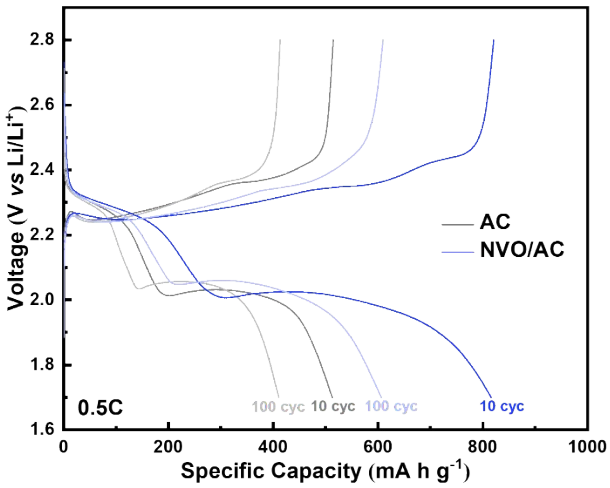

Fig. S12 Voltage profiles of AC and NVO/AC at the 10th and 100th cycles (0.5C).

Table S1. Comparison of the electrochemical performance of the NVO/AC composite with previously reported vanadium-based sulfur host materials for Li–S batteries.

Material	Initial capacity (mA h g^{-1})	Cycle number, retention	Ref.
V_2O_5@N-MWCNTs	1453 (@ 0.1C)	200 cycles, 0.5C, 60%	S1
V_2O_5	1209 (@ 0.1C)	100 cycles, 0.2C, 87%	S2
VO_2-VS_2	1236 (@ 0.2C)	500 cycles, 1C, 50.6%	S3
rGO-VS_2/S	1289.3 (@ 0.1C)	200 cycles, 0.2C, 77.8%	S4
NVO/AC	1476.96 (@ 0.1C)	300 cycles, 0.5C, 59.4%	This work

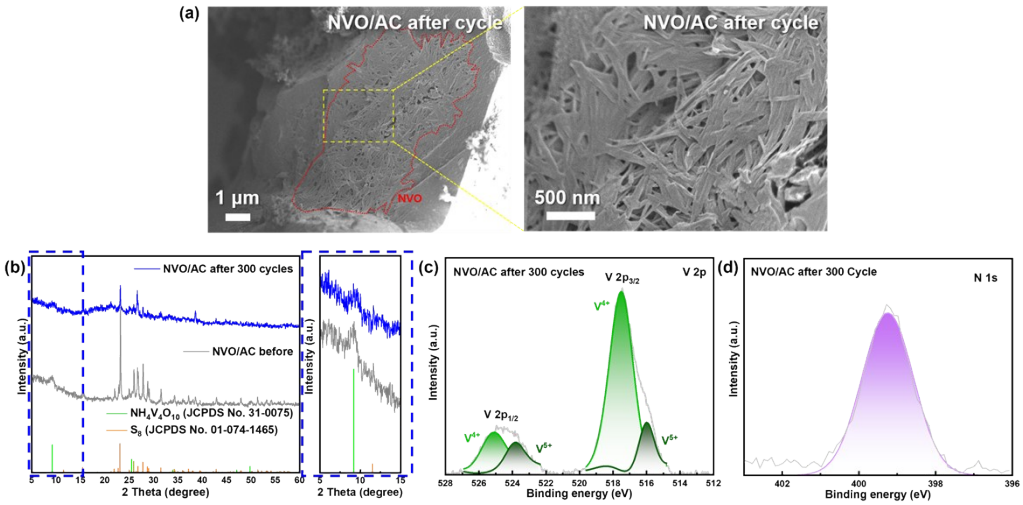

Fig. S13 (a) XRD pattern graphs of before and after 300 cycles at 0.5 C. XPS spectra (b) V 2p and (c) N 1s of NVO/AC after 300 cycles.

Supporting equations

A. Beweick, M. Fleischman, and H.R Thirsk (BFT) Model

2D Instantaneous inucleation (2DI)	2D Progressive nucleation (2DP)
$\frac{i}{i_m} = \left(\frac{t}{t_m}\right)\left\{exp\left[\frac{t^2 - t_m^2}{2t_m^2}\right]\right\}$	$\frac{i}{i_m} = \left(\frac{t}{t_m}\right)\left\{exp\left[\frac{-2\left(t^3 - t_m^3\right)}{3t_m^3}\right]\right\}$
(S1)	(S2)

Scharifker-Hills (SH) Model

3D Instantaneous nucleation (3DI)	3D Progressive nucleation (3DP)
$\frac{i}{i_m} = \left(\frac{1.9542}{t/t_m}\right)^{1/2}\left\{1 - exp\left[1.2564\left(\frac{t}{t_m}\right)\right]\right\}$	$\frac{i}{i_m} = \left(\frac{1.2254}{t/t_m}\right)^{1/2}\left\{1 - exp\left[2.3367\left(\frac{t}{t_m}\right)^2\right]\right\}$
(S3)	(S4)

Where I_p represents maximum peak current, t_m represents the time corresponding the current reach the maximum current.[S5]

References

S1. C. Liu, M. Xiang, H. Zhang, S. Feng, J. Xiao, S. Ma and X. Li, Preparation and Electrochemical Performance of V_2O_5 @N-CNT/S Composite Cathode Materials, *Frontiers in Energy Research*, 2021, **8**, 615558.

S2. R. Carter, L. Oakes, N. Muralidharan, A. P. Cohn, A. Douglas and C. L. Pint, Polysulfide Anchoring Mechanism Revealed by Atomic Layer Deposition of V_2O_5 and Sulfur-Filled Carbon Nanotubes for Lithium–Sulfur Batteries, *ACS Appl. Mater. Interfaces*, 2017, **9**, 7185-7192.

S3. T. Zhang, C. Zha, S. Liu and L. Zhou, Boosting the polysulfide conversion by VO_2-VS_2 heterostructure for lithium-sulfur batteries, *J. Alloys Compd.*, 2023, **955**, 170285.

S4. Z. Cheng, Z. Xiao, H. Pan, S. Wang and R. Wang, Elastic Sandwich-Type rGO–VS_2/S Composites with High Tap Density: Structural and Chemical Cooperativity Enabling Lithium–Sulfur Batteries with High Energy Density, *Adv. Energy. Mater.*, 2017, **8**, 1702337.

S5. J. Sun, Y. Liu, L. Liu, J. Bi, S. Wang, Z. Du, H. Du, K. Wang, W. Ai and W. Huang, Interface Engineering Toward Expedited Li(2) S Deposition in Lithium-Sulfur Batteries: A Critical Review, *Adv. Mater.*, 2023, **35**, e2211168.